ELSEVIER

Chemical Geology 209 (2004) 327–340

CHEMICAL GEOLOGY
INCLUDING
ISOTOPE GEOSCIENCE

www.elsevier.com/locate/chemgeo

H_2O diffusion in dacitic melts

Yang Liu[a,*], Youxue Zhang[a], Harald Behrens[b]

[a]*Department of Geological Sciences, University of Michigan, Ann Arbor MI 48109, USA*
[b]*Institut für Mineralogie, Universität Hannover, Callinstr. 3, D-30167 Hannover, Germany*

Received 5 June 2003; accepted 17 June 2004

Abstract

We report the first experimental study of the diffusion of H_2O in dacitic melts. Dehydration experiments were conducted at 551–637 °C and 1–1450 bars for samples with ~0.8 to ~2.5 wt.% total dissolved H_2O. The H_2O diffusivity is proportional to total H_2O contents at ≤0.8 wt.%, but increases exponentially with total H_2O at higher H_2O contents. The diffusivity of the total dissolved H_2O (in $\mu m^2/s$) can be modeled as

$$D_{H_2O_t} = X\exp[20.463 - 40.433X + (-18,106 + 69,230X)/T],$$

where X is the mole fraction of the total dissolved H_2O on a single oxygen basis and T is in Kelvin. In the investigated T-range, H_2O diffuses more slowly in hydrous dacitic melt than in rhyolitic melt, by a factor of 2 to 12. When compared to H_2O diffusion in rhyolite, the activation energy in dacite is greater (124–142 vs. 87–91 kJ/mol). Therefore, extrapolation of $D_{H_2O_t}$ in dacite to higher T suggests that above certain T, H_2O diffusivity in dacite would be greater than that in rhyolite (e.g., at >740 °C and 100 MPa for a total H_2O content of 2.5 wt.%).

Keywords: Water diffusion; Dacitic melt; Bubble growth; Magma fragmentation

1. Introduction

Understanding H_2O diffusion in magma is crucial to the understanding of bubble growth, magma degassing and volcanic eruptions. In addition to large caldera-forming eruptions composed of mainly rhyolitic magmas, many explosive dacitic eruptions exist (either dacitic in terms of whole rock composition such as Unzen Volcano, Japan or andesitic with dacitic melt composition such as Redoubt Volcano, Alaska, USA) (Swanson et al., 1994; Wolf and Eichelberger, 1997; Nakada and Motomura, 1999). The study of H_2O diffusion in these melts is necessary to model such volcanic eruptions.

The diffusion of H_2O has long been studied in glass sciences (e.g. for silica glass by Doremus, 1962, 1983). In natural melts, only the rhyolitic melt has been

* Corresponding author. Current address: Department of Geophysical Sciences, University of Chicago, 5734 South Ellis Avenue, Chicago, IL 60637, USA.
E-mail address: yangl@geosci.uchicago.edu (Y. Liu).

0009-2541/$ - see front matter © 2004 Elsevier B.V. All rights reserved.
doi:10.1016/j.chemgeo.2004.06.019

studied extensively (Shaw, 1974; Friedman and Long, 1976; Delaney and Karsten, 1981; Karsten et al., 1982; Lapham et al., 1984; Zhang et al., 1991; Nowark and Behrens, 1997; Zhang, 1999; Zhang and Behrens, 2000). Shaw (1974) demonstrated that H_2O diffusivity strongly depends on total dissolved H_2O content (hereafter referred to as H_2O_t), which was further verified by Delaney and Karsten (1981) and Lapham et al. (1984). Zhang et al. (1991) modeled H_2O diffusion in rhyolitic melts by considering the role of H_2O speciation and concluded that molecular H_2O (hereafter referred to as H_2O_m) is the diffusion species, and hydroxyl group is immobile and its concentration varies due to the species reaction. Nowark and Behrens (1997) showed that at high H_2O_t for a haplogranitic melt (compositionally similar to natural rhyolite used by Zhang et al., 1991), H_2O_t diffusivity increases much more rapidly with increasing H_2O_t content than extrapolation using the model of Zhang et al. (1991). Zhang and Behrens (2000) extended the study of H_2O in rhyolitic melts to high pressure (8.1 kbars), high temperature (1200 °C) and high H_2O_t contents (7.7 wt.%). They found that H_2O_m diffusivity depends exponentially on H_2O_t, which reconciles diffusion data at both low and high H_2O_t, and developed a model to calculate water diffusivity in rhyolitic melts for a wide range of geological situations. Experimental investigations on other natural melt compositions are scarce. Zhang and Stolper (1991) studied a basaltic melt with H_2O_t of 0.2–0.4 wt.% at 1.0 GPa and 1300–1500 °C and Freda et al. (2003) a potassium-rich trachyte with 0.25–2 wt.% H_2O at 1.0 GPa, 1100–1400 °C. To remedy the lack of diffusion data for melts of intermediate composition between rhyolite and basalt, here, we report the first experimental study of H_2O diffusion in dacitic melts.

2. Experimental and analytical methods

2.1. Starting materials

Anhydrous dacite with a composition similar to Unzen dacite (Table 1) was synthesized by fusing oxides and carbonates at 1600 °C in air (Ohlhorst et al., 2001). Syntheses of hydrous samples with 0.8–2.5 wt.% H_2O_t were performed in a conventional internally heated pressure vessel (IHPV) at 1250 °C and 3–5 kbars for 13–48 h. The intrinsic oxygen fugacity in the IHPV is high if water activity in the experimental charge equals one ($\Delta NNO \approx +3$, close to the MnO–Mn_3O_4 buffer, Berndt et al., 2002). Due to the water formation reaction $H_2+1/2O_2=H_2O$, oxygen fugacity is lower if the melt is water-undersaturated as in our syntheses (capsule walls are permeable to hydrogen but not to oxygen). To obtain large pieces of homo-

Table 1
Composition of dacitic glass for diffusion experiments (wt.%)

	DC2B original	DC53b2 637 °C, ~5.5 days	DC2B4 608 °C, 11 h	DC2B2 507 °C, ~18 days
SiO_2	65.03±0.27	65.92±0.26	65.48±0.26	64.96±0.26
TiO_2	0.67±0.07	0.62±0.04	0.65±0.04	0.63±0.04
Al_2O_3	16.63±0.13	15.58±0.14	16.40±0.14	16.63±0.15
FeO_T	4.16±0.14	4.33±0.11	4.46±0.11	4.43±0.11
MgO	1.96±0.06	2.24±0.05	2.00±0.05	2.00±0.05
CaO	5.10±0.09	4.66±0.08	5.11±0.08	4.93±0.08
Na_2O	3.95±0.24	3.64±0.18	4.04±0.2	4.03±0.19
K_2O	2.70±0.08	2.56±0.06	2.62±0.06	2.58±0.06
H_2O_t	2.4	0.48–0.75[a]	2.5	0.5–2.4[a]
Total	100.20	99.56	100.76	100.19
*N**	7	4	3	4

**N* is the number of microprobe analyses. The molar weight of anhydrous dacitic melt on a single oxygen basis is 33.82 g/mol. Electron microprobe analyses (EMPA) were conducted with an electron microprobe (Cameca MBX) using a defocused beam (~6 μm) with 3–4 nA current. Oxide contents of each sample were normalized to anhydrous composition (microprobe results/$(1-c)$, where c is the H_2O_t content obtained using FTIR). Error (1σ) of the analysis is shown.

[a] H_2O_t contents were determined using FTIR spectroscopy and the calibration of Ohlhorst et al. (2001). For samples after experiments, EMPA were conducted on the same wafers used for FTIR analyses. Only the center of the sample DC2B4 was analyzed using EMPA, where H_2O_t contents are not affected by diffusion. EMPA were also done on the region affected by diffusion for samples DC53b2 and DC2B2.

geneous hydrous glass (0.6–0.8 g), powdered anhydrous glass and water were loaded into a $Au_{80}Pd_{20}$ capsule (3 mm in diameter and 30 mm in length) in turn in several portions. The packing of loaded powders affected the dissolved air contents in the synthetic sample (which may help bubble formation, see later discussion). At the end of the experiment, samples were quenched under isobaric conditions. The synthetic samples are roughly elliptical cylinders with a short axis diameter of 2–3 mm, long axis diameter of 3.4–5 mm and a length of about 30 mm. Polished pieces of the synthesized hydrous glass (usually from glass in contact with the capsule or at the two ends) are light brown in color and contain no quench crystals or bubbles. Microprobe analyses do not show significant heterogeneity that would indicate Fe loss. A section of 1–3 mm thick was cut from the synthesized sample and doubly polished for diffusion experiments.

2.2. Experimental methods

Table 2 lists experimental conditions. Nine dehydration experiments were conducted for 0.8–2.5 wt.% $H_2O_{t,i}$ (the subscript i refers to initial concentration) at 500–600 °C under Ar pressure of ~0.9 to ~1.4 kbars (to prevent bubble formation). Two rapid-quench cold-seal vessels (CSV-1 at Universität Hannover and CSV-2 at the University of Michigan) were used. CSV-1 is made by a Ni-rich alloy and the imposed oxygen fugacity is close to NNO+2.3 if argon is used as the pressure medium and water activity in a capsule equals to one (Berndt et al., 2001). CSV-2 is made of TZM alloy (titanium zirconium molybdenum). Pressure medium in CSV-2 is purified Ar. One dehydration experiment (DC53b3) was conducted at 550 °C and 1 bar in a horizontal tube furnace using a sample containing ~0.74 wt.% $H_2O_{t,i}$.

For experiments conducted in CSV-1, a piece of doubly polished dacitic glass (2 mm in short axis, 5 mm in long axis and ~2 mm in thickness) was placed side by side with hydrous andesitic and Fe-free andesitic glasses in an open gold capsule (results for andesitic glasses will be reported elsewhere). The capsule was clamped into a groove at the tip of a Ni rod. The sample and rod were then placed in CSV-1 and brought to the specified temperature and pressure. During the experiment, temperature was monitored using a sheathed type K thermocouple outside the autoclave and usually varied by ±2 °C. The uncertainty in temperature, including that associated with the uncertainty in sample position, was estimated to

Table 2
Experimental conditions of dehydration experiments

Experiments	T (°C)	P (bars)	Durations[a] (s)	$H_2O_{t,i}$ (wt.%)	Best a[b]	r^2[b]	Apparatus	Comments[c]
DC2B5	637±10	1314–1338	19,660	2.4–2.5	50	0.9983	CSV-2	b
DC2B4	608±10	1450–1400	40,878	2.45	55	0.9991	CSV-2	b
DC2B1[d]	605±5	1030–340	103,975	2.4–2.5	nd	nd	CSV-1	not used, b
DC2A3	561±5	1020–980	689,315	2.4–2.5	60	0.9983	CSV-1	b
DC2B2[d]	507±5	1030–1010	1,554,510	2.4–2.5			CSV-1	not used, b, x
DC2A1[d]	503±5	1030±5	172,200	2.4–2.5	nd		CSV-1	
DC1	608±10	970–940	180,900	1.4–1.5	nd		CSV-2	not used, b
DC53b2	638±10	990	484,260	0.73	nd		CSV-2	
DC53b1	608±10	975–927	413,880	0.75	nd		CSV-2	
DC53b3[e]	551±10	1	1,744,680	0.74	nd			

[a] Experimental durations are not corrected for heating and quenching time, which are insignificant compared to the long duration of the experiments. The estimated heating up time is about 30 min in CSV-1 and few minutes in CSV-2.

[b] Results of best-fit a values by fitting diffusion profiles assuming $D_{H_2O_m}=D_0\exp(aX)$. R^2 is the quality of the fitting.

[c] b: bubbles, x: crystallization.

[d] These samples are not used in obtaining diffusivity data. For sample DC2B1, the pressure dropped from 1030 to 340 bars during the course of the experiment. Crystallization may occur in sample DC2B2. H_2O diffusion profile in DC2A1 is too short for extracting H_2O diffusivity.

[e] This experiment was conducted in 1-bar horizontal tube furnace.

be ±5 °C. The heating duration was <40 min (Zhang and Behrens, 2000) and rapid quench was accomplished by turning the furnace to vertical position, dropping the sample to the cool dense Ar atmosphere. The estimated quench rate is ~30 °C/s at 2 kbars (Zhang et al., 2000).

For experiments conducted in CSV-2, a piece of doubly polished dacitic glass was wrapped in wires or a piece of Au foil, and was then fixed at the top of a steel elevator rod. The steel elevator rod sat on an iron rod and then both were placed into the cold part of CSV-2. The pressure vessel was heated to desired temperature. After the temperature stabilized, the sample was raised into the hot spot by lifting the elevator rod with an electromagnet. Temperature was monitored during experiments using a sheathed type K thermocouple located outside the vessel and at the same position as the top of the vessel. During experiments, the outside temperature varied by <1 °C. The temperature gradient inside the furnace was ~2 °C/mm within 6 mm of the hotspot, tested using a piece of hydrous obsidian and the H_2O speciation model of Zhang et al. (1997). The uncertainty in temperature, including that associated with the sample position, was estimated to be about 10 °C. The time needed for heating up the sample was short (heating rate was roughly 100 K/s, see below for quench rate) and hence there was no need to correct for the experimental duration. At the end of the experiments, rapid quench was achieved by turning off the power to the electromagnet, dropping sample to the cool dense Ar atmosphere. During quench, the pressure of the system initially increased by >20 bars, which indicates the operation was successful. A quench rate of 100–200 °C/s was estimated using a piece of obsidian glass with 0.8 wt.% H_2O_t and the geospeedometer of Zhang et al. (2000).

For the experiment conducted in the 1-bar horizontal tube furnace, the furnace was first heated to the desired temperature. Temperature gradient was about 0.2 °C/mm within 5 mm of the hot spot. The sample (0.74 wt.% $H_2O_{t,i}$) was put in an Au holder and placed at the hotspot adjacent to a Pt-$Pt_{90}Rh_{10}$ thermocouple. Temperature measured by the Pt-$Pt_{90}Rh_{10}$ thermocouple first decreased and gradually became stable at the desired temperature in <3 min. The sample was exposed in air during experiment. Quench was achieved by taking the sample out and cooling it in air.

2.3. FTIR

Concentrations of H_2O_t and of each species (H_2O_m and OH) for these samples were determined using Fourier transform infrared spectroscopy (FTIR). Starting samples were analyzed in the main chamber of a Perkin-Elmer Spectrum FTIR GX spectrometer using a visible source, a CaF_2 beamsplitter and a liquid-N_2 cooled InSb detector. The main chamber was purged with dry N_2 during analyses. A round aperture (531 μm in diameter) was placed between the source and the sample. Measurements showed that starting samples were homogeneous in H_2O_t within 5% relative, except for samples with ~0.8 wt.% H_2O_t (up to 19% relative). After experiments, a thin wafer perpendicular to the originally polished surfaces was cut and doubly polished to a thickness of 100–270 μm. To obtain the diffusion profile, these thin wafers were placed on an automated stage of a microscope attached to the Perkin-Elmer Spectrum FTIR GX. Analytical conditions included a visible source, a CaF_2 beamsplitter, a liquid-N_2 cooled MCT detector, a slit aperture (10–20 μm wide and 400–800 μm long), 64 or 128 scans and a gain of 1 or 2. Samples were in contact with air during microscope IR analyses. To minimize interference from atmospheric CO_2 and H_2O, a new background was taken after every two or three analyses. A few samples (DC53B2, DC1 and DC2A3) were also analyzed in the main chamber to check the consistency between main chamber and microscope analyses. The H_2O_t contents at the center (not affected by diffusion) determined using main chamber and microscope agree with each other within 10% relative.

In order to obtain the H_2O_t concentration, peak heights were used after subtracting the baseline of the spectrum. The H_2O_t concentration of all starting samples and samples after experiments with $H_2O_{t,i}$> 1.4 wt.% was determined using the calibration of Ohlhorst et al. (2001) for dacitic melt. For all starting samples, which were synthesized at similar conditions as those in the calibration of Ohlhorst et al. (2001), the baseline of the spectrum was fit with two straight lines (TT method in Ohlhorst et al., 2001). However, for samples after experiments, the spectrum shape changed and the Fe^{2+} band at 5600 cm^{-1} disappeared (Fig. 1). For those samples with $H_2O_{t,i}$>1.4 wt.%, the baseline of the spectrum was also fit using two straight lines. Because of the difference in the shape of the

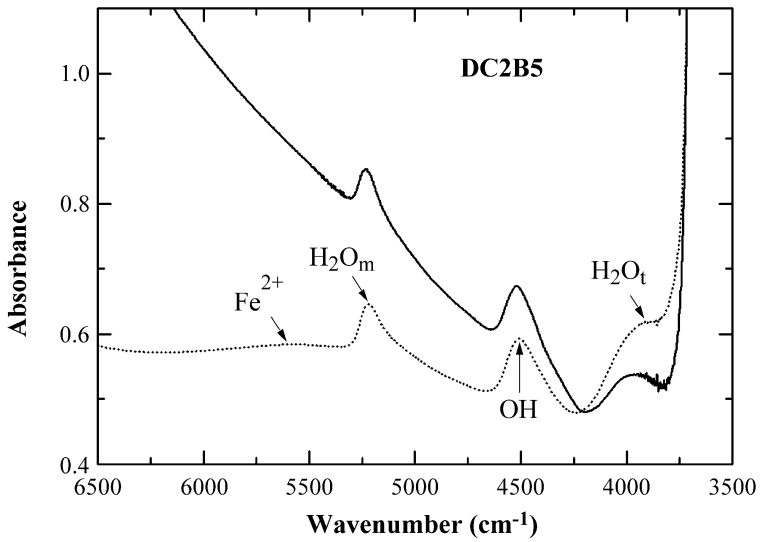

Fig. 1. FTIR spectra of sample DC2B5 before (dotted curves) and after experiments at 637 °C (solid curves) normalized to a thickness of 0.5 mm. The spectrum after experiment was taken in the center of the sample where H_2O_t is not affected by diffusion.

spectrum, there is inaccuracy in using the calibration of Ohlhorst et al. (2001) to determine H_2O_t for samples with altered baseline shape (see discussion below). For experimental charges with ~0.8 wt.% $H_2O_{t,i}$, owing to the low H_2O_t content, the absorption band for H_2O_m (~5200 cm^{-1}) is indistinguishable from the baseline after experiments. Subtracting a linear baseline can result in a zero or even negative peak intensity. Therefore, the absorption band at 3570 cm^{-1} was used and its baseline was fit with a flexicurve. An absorption coefficient of 68 l/mol/cm from Yamashita et al. (1997) was used to obtain the H_2O_t.

2.4. Analytical methods for glass composition

Glass compositions of a few samples after experiments (FTIR wafers from experiments DC2B4, DC2B2 and DC53b2) were analyzed using a Cameca MBX electron microprobe. Compositions of these samples agree with original samples within 2σ errors (Table 1). The double-polished wafers used for FTIR analyses from several samples (DC2B1, DC2A3, DC2B2, DC2B5, DC1, DC53b3, DC53b1 and DC53b2) were also checked using a Hitachi S-3200N scanning electron microscope (SEM). Bubbles with a diameter of about 0.7 μm were found in samples DC2 and DC1, but no bubbles were seen in the DC53 samples. The approximate distance between closest bubbles is ~10 μm. In general, there is no discernable difference in bubble distribution except for the sample DC2B1, in which there is a bubble-free layer of ~10 μm thick close to the originally polished surfaces. No obvious crystallization was observed.

3. Results

Ten experiments were conducted, of which seven are deemed successful. The experimental conditions for all experiments are listed in Table 2. The concentration profiles are shown in Fig. 2. For one discarded experiment (DC2B1), the pressure dropped from 1030 to 340 bars during the course of the experiment. For the other discarded experiment (DC2B2), there is indication of significant crystallization (see below). Diffusion profiles in the third discarded experiment (DC2A1) are too short to obtain diffusivity.

One complexity is possible devitrification in samples because experimental temperatures were below the liquidus. No significant crystallization was observed in any samples using the scanning electron microscope. However, a noticeable shoulder appears at ~4300 cm^{-1} in the IR spectra of the DC2B2 sample. This shoulder band is roughly at the same wavenumbers as the combinational OH band in mica

(Rossman, 1984). Two samples (DC2B2 and DC2B5) and the original DC2 sample were checked using a transmission electron microscope. The original sample DC2 and sample DC2B5 appear similar with no noticeable crystallization. In the DC2B2 sample, few elongated crystals about 6 nm wide and 38 nm long were observed, but they cannot be identified. Potential hydrous minerals are biotite and amphibole. To be on the safe side, sample DC2B2 is disregarded.

Complexities in the experiments also include change in IR spectrum and bubbles in samples DC2A, DC2B and DC1. However, these complexities cause small uncertainties in determined H_2O diffusivity (see discussion below). With these complexities in mind, the best diffusion profiles are obtained from samples DC2B5, DC2B4, DC1, DC53b1 and DC53b3.

4. Discussion

4.1. Modeling the diffusivity of H_2O

The experimental temperature is always close to the glass transition temperature (T_g), which can be inferred

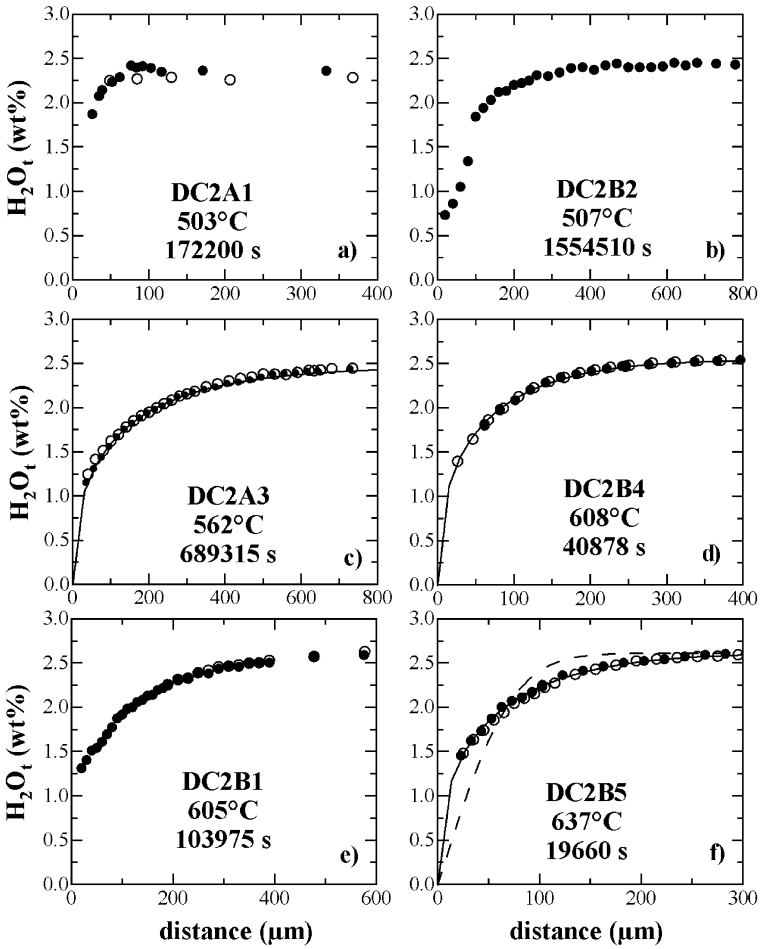

Fig. 2. Diffusion profiles of H_2O in dacitic melt. Two profiles were obtained from each sample except DC2B2 and DC1. Filled circles are for one profile and open circles for the other. Some data points far away from the edge are not shown so that data and the fit are shown more clearly. Solid curves are fits to filled circles using a from Eq. (2) and D_0 in Table 3. Dotted curves are fit to open circles. Dashed curves in (f) and (j) are error function curves. All experimental profiles were adjusted for Δx_0 (see text and Table 3).

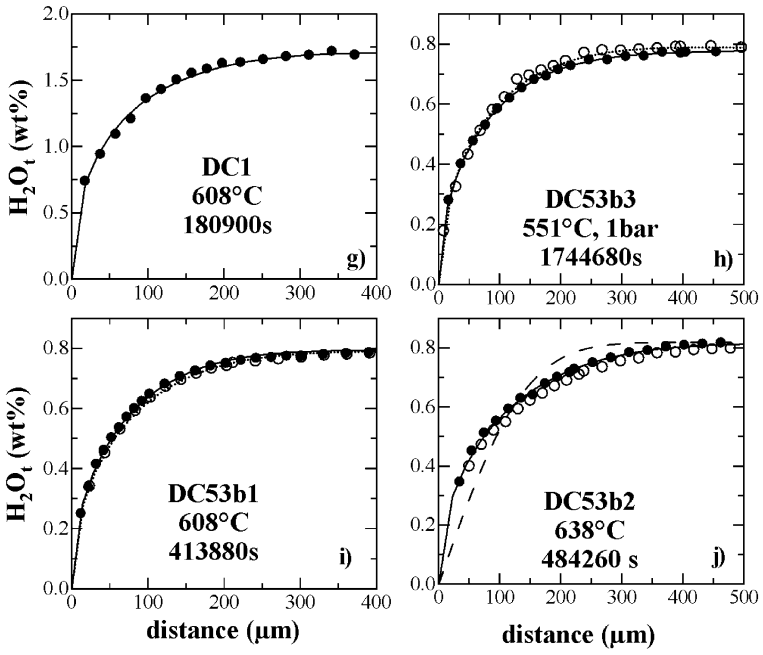

Fig. 2 (*continued*).

using logη (at T_g)=11.45−log|q|, where the viscosity (η) is in Pa·s and q is the quench rate in °C/s (Zhang et al., 2003). Because viscosity of hydrous dacitic melt has not been investigated, T_g is estimated from viscosity models of trachyte (Whittington et al., 2001), and from averaging log η of andesite (Richet et al., 1996) and rhyolite (Zhang et al., 2003). During the diffusion experiment, assuming q<5 °C/duration where 5 °C is the maximum variation in temperature over the duration of an experiment, the calculated T_g is below the experimental temperature. That is, the sample was in the melt state based on the calculation. During quench, the sample was in the glass state based on similar calculation.

The H_2O_t content at the edge of the sample (i.e., surface H_2O_t) cannot be directly measured but is expected to be zero. We carried out one 1-bar experiment and seven CSV experiments. Zhang et al. (1991) verified that, for 1-bar experiments in rhyolite, the surface concentration is essentially zero. Our 1-bar experiment followed their procedure except that during our experiment there was no dry N_2 gas stream. The H_2O solubility at the surface of the sample is <0.019 wt.% estimated using a partial water pressure in air of 10–20 mbars and the solubility model for rhyolitic melt from Liu et al. (2004a). For experiments conducted in CSV, f_{H_2O} during the experiment is negligible (estimated to be <0.03 bar even accounting for H_2O content in the sample), implying near-zero H_2O_t (e.g., <0.02 wt.%) at the surface. Furthermore, surface H_2O_t content due to the presence of water vapor in the apparatus should depend only on experimental temperature and f_{H_2O}, and be independent of $H_2O_{t,i}$. In our data, samples with different $H_2O_{t,i}$ at same temperature (such as DC2B5 and DC53B2 in Fig. 2f and j) show different near-surface H_2O concentrations (first measurable point close to the edge, usually 20–30 μm away from the edge), consistent with non-zero near-surface H_2O_t contents resulting from the spatial resolution of the IR microscope. Moreover, measured concentration profiles show H_2O_t contents at surface are near zero (e.g. Figs. 2h and i).

One might argue that if surface concentration is allowed to be a fit parameter, the diffusion profile may be fit by an error function (i.e., concentration-independent diffusivity). Although this argument is mathematically true for each single profile, when error

function fitting is applied to profiles with different $H_2O_{t,i}$ but otherwise similar experimental conditions, very different diffusivities would be obtained. For example, fitting an error function, diffusivity for DC2B5 (637 °C, 2.6 wt.% $H_2O_{t,i}$) would be eight times greater than that for DC53b2 (638 °C, 0.76% $H_2O_{t,i}$), demonstrating that diffusivity must depend strongly on H_2O_t content. The surface H_2O_t would also depend on the experiment (1.4% for DC2B5 and 0.36% for DC53b2). Thus, fitting the diffusion curve by allowing surface concentration to be a fit parameter and by assuming diffusivity is independent of H_2O_t would lead to self-inconsistency in both diffusivity values and surface concentrations among different samples.

Assuming the surface concentration is essentially zero, the measured concentration profiles deviate significantly from error function curves, demonstrating that the diffusivity of H_2O in dacitic melt depends strongly on H_2O_t contents (a conclusion that would be reached even when D for individual profile is assumed to be constant, see above), similar to results in rhyolitic melt (Zhang and Behrens, 2000). Preliminary data fitting using the method of Zhang et al. (1991) and Zhang and Behrens (2000) shows that the diffusivity of H_2O_t is proportional to H_2O_t at H_2O_t contents ≤0.8 wt.%, but increases exponentially at greater H_2O_t. This observation is similar to that for H_2O diffusion in rhyolite, although for rhyolites the linear region is up to 2 wt.% H_2O_t. Hence, the diffusion mechanism in dacitic melts is inferred to be similar to that in hydrous rhyolitic melts with H_2O_m being the diffusing species and $D_{H_2O_m}$ increasing exponentially with H_2O_t (Zhang et al., 1991; Zhang, 1999; Zhang and Behrens, 2000). In addition, that the diffusivity of a molecular species (such as H_2O_m) increases exponentially with H_2O_t has been confirmed by a recent Ar diffusion study on rhyolitic glasses and melts (Behrens and Zhang, 2001).

To model the dependence of H_2O diffusivity on H_2O contents, a forward approach that employs a functional relation between diffusivity and H_2O_t is used to fit the profiles (Zhang and Behrens, 2000). Because all experiments were conducted at relatively low pressures (1–1450 bars), the pressure effect is not expected to be resolvable (Zhang and Behrens, 2000) and thus is ignored. In the fit, it is assumed that (i) the H_2O_t content is zero at sample surface, (ii) H_2O_m is the diffusing species and (iii) there is local species equilibrium between H_2O_m and OH:

$$K = [OH]^2/\{[H_2O_m][O]\} = \exp(2.88 - 3567/T) \quad (1)$$

and (iv) the dependence of $D_{H_2O_m}$ on H_2O_t can be expressed as

$$D_{H_2O_m} = D_0 \exp(aX), \quad (2)$$

where D_0 is $D_{H_2O_m}$ as H_2O_t concentration approaches zero and X is the mole fraction of H_2O_t on a single oxygen basis, a is a constant. Both D_0 and a values depend on T but are independent of X. Liu et al. (2004b) show that equilibration between H_2O_m and OH is reached in <2 min for samples with 2.5 wt.% H_2O_t at 537 °C and <6 min for samples with 1.5 wt.% H_2O_t at 519 °C. At higher temperatures (600 and 637 °C), the reaction rate is faster. The time scale of species conversion is fast compared to the experimental time scale and, hence, local equilibrium of water speciation is justified. There are two fitting steps. The first step is to fit individual profiles to constrain the parameter a. After this step, for self-consistency, a formula describing a as a function of T is obtained and then all the profiles are refit to constrain D_0 as a function of T.

We do not have a program to fit a profile to obtain simultaneously a and D_0 values. Hence, a is obtained by trial and error. For a given experimental profile, a in Eq. (2) is given to calculate a theoretical profile and the actual profile is fit by the theoretical profile (which shows how the concentration should vary with x and t) to obtain D_0 and Δx_0 (the adjustment of the interface position) using the program of Zhang and Behrens (2000). The value of Δx_0 would be zero if everything were perfect, but it can be nonzero due to (i) imperfect cut of the wafer (not perfectly vertical to original surface), (ii) chipping at the edge and (iii) error in determining the distance from surface. Nevertheless, the absolute value of Δx_0 should be close to zero and should be less than 20 μm.

Then, other a values are given and the fit is repeated. The best fit (with highest r^2) among the group of fits constrains the a value for the profile. However, the a value obtained from one single profile may have large uncertainty. Hence, in our work, constraints for obtaining the best-fit a value also

include the following: (i) the calculated curve can well fit the shape of individual profiles, especially for samples with ~2.5 wt.% H_2O_t, and (ii) roughly the same pair of (a, D_0) values can be used to fit profiles at the same T and P but with different $H_2O_{t,i}$ (e.g., experiments DC2B4, DC1 and DC53b1 at 608 °C as one group, DC2B5 and DC53b2 at 637 °C as another group). The best-fit a values are listed in Table 2. From these initial fitting, a values can be expressed as:

$$a = -(58\pm17) + (99,000\pm15,300)/T, \quad (3)$$

where T is in Kelvin. Note that this equation is based on three profiles because the procedure to obtain the best-fit value is very time consuming.

Then, all experimental diffusion profiles were refit to obtain D_0 using a values from Eq. (3). The quality of the fit of all profiles using Eq. (2) is high (Fig. 2). The D_0 and Δx_0 values are presented in Table 3. In most cases, Δx_0 values from the fit are within the spatial resolution of the IR microscope. After adjusting Δx_0, all experimental diffusion profiles with fits are plotted in Fig. 2. The D_0 values are plotted in Fig. 3 and its temperature dependence can be expressed as:

$$\ln D_0 = (20.298\pm0.934) - (20,661\pm814)/T, \quad (4)$$

where D_0 values are in $\mu m^2/s$ and T is in Kelvin. This equation reproduces experimental ln D_0 values to within 0.21 (equivalent to 23% precision in D_0 values). From Eqs. (2), (3) and (4), $D_{H_2O_m}$ can be expressed as:

$$D_{H_2O_m} = \exp[20.298 - 58.217X + (-20,661 + 98,995X)/T]. \quad (5)$$

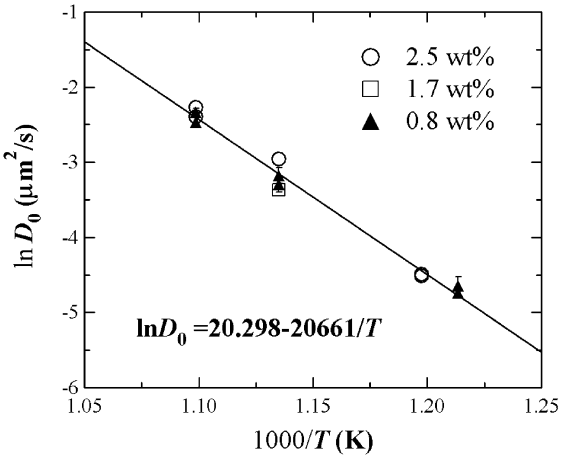

Fig. 3. The dependence of ln D_0 on 1/T. Fitting errors (2σ) of ln D_0 values are plotted if greater than the symbol size.

The activation energy decreases from 160 kJ/mol at 0.8 wt.% H_2O_t to 134 kJ/mol at 2.5 wt.% H_2O_t.

With the relationship in Eq. (5) and the equilibrium speciation of H_2O, the diffusivity of H_2O_t ($D_{H_2O_t}$) may be calculated using

$$D_{H_2O_t} = D_{H_2O_m} dX_m/dX, \quad (6)$$

where X_m is the mole fraction of H_2O_m (Zhang et al., 1991). Using Eqs. (5) and (6) and the speciation

Table 3
Results for ln D_0 by fitting diffusion profiles assuming $D_{H_2Om}=D_0\exp(aX)$, where $a=-58+99{,}000/T$ (T is in Kelvin)

Experiments	T (C)	P (bars)	H_2O_t[a] (wt.%)	H_2O_t[b] (mole fraction)	ln D_0[c] (μm^2/s)	Δx_0 (μm)	r^2
DC2B5.1[d]	637±10	1314–1338	2.61	0.0479	−2.40±0.05	6.69	0.9982
DC2B5.2	637±10	1314–1338	2.61	0.0479	−2.27±0.06	14	0.9979
DC2B4	608±10	1450–1400	2.54	0.04665	−2.96±0.06	14.1	0.998
DC2A3.1[d]	561±5	1020–980	2.34	0.04305	−4.49±0.04	15.21	0.9983
DC2A3.2[d]	561±5	1020–980	2.36	0.04341	−4.51±0.06	21.14	0.9965
DC1	608±10	970–940	1.76	0.03254	−3.36±0.12	1.13	0.995
DC53b2.1	638±10	950–990	0.82	0.01528	−2.47±0.06	14.09	0.9978
DC53b2.2	638±10	950–990	0.78	0.01454	−2.33±0.05	21.01	0.9987
DC53b1.1[d]	608±10	975–927	0.77	0.01436	−3.29±0.05	2.01	0.9981
DC53b1.2[d]	608±10	975–927	0.77	0.01436	−3.18±0.07	3.62	0.9975
DC53b3.1	551±2	1	0.75	0.01399	−4.74±0.03	−3.77	0.9993
DC53b3.2	551±2	1	0.79	0.01473	−4.64±0.12	−11.59	0.9914

[a] The H_2O_t content at the center of the sample was used in fitting.
[b] Mole fraction of H_2O_t on a single oxygen basis calculated using the molar weight of 33.82 g/mol for anhydrous dacitic melt.
[c] Fitting error is given at 2σ level.
[d] Two profiles were measured for these samples and both are used to obtain D.

model (Eq. (1)), $D_{H_2O_t}$ is calculated for H_2O_t contents ≤2.5 wt.%.

An expression of $D_{H_2O_t}$ is then obtained:

$$D_{H_2O_t} = X\exp[20.463 - 40.433X + (-18,106 + 69,230X)/T], \quad (7)$$

where $D_{H_2O_t}$ is in $\mu m^2/s$. Eq. (7) reproduces $D_{H_2O_t}$ values from Eqs. (4) and (5) within 6% at 500–640 °C and 0.6–2.6 wt.% H_2O_t. Combining the fit error of 0.21 in ln D_0 in Eq. (4), and the 6% error in producing Eq. (7), the fit error in ln $D_{H_2O_t}$ is 0.22. Furthermore, because of large uncertainty in speciation models for dacitic melt (Liu et al., 2004b), Eqs. (3) to (5) do not have much physical meaning and only serve the purpose for deriving Eq. (7).

When $D_{H_2O_t}$ exponentially depends on X, a values are best constrained using either diffusion couple experiments or dehydration experiments with high H_2O_t (Zhang and Behrens, 2000). Because the temperature and H_2O_t content covered by this work are limited, caution should be exercised to extrapolate to other T-H_2O_t conditions, especially when extrapolating to high H_2O_t.

4.2. Uncertainties in H_2O_t diffusivity

One uncertainty in inferred H_2O_t diffusivity is related to the change of spectrum baseline. First, there may be a systematic error in determining H_2O_t contents using the calibration of Ohlhorst et al. (2001) because the shape of the IR spectra for samples after experiments is different from that for the calibration study of Ohlhorst et al. (2001). Compared with H_2O_t contents before experiments analyzed in the main chamber, those in the center of the samples after experiments (unaffected by diffusion) analyzed using the IR microscope increased apparently by up to 9% for the DC2 samples and by 18% for the DC1 sample. The H_2O_t contents obtained using IR microscope are not corrected for the difference. Although the lack of an accurate calibration of the IR bands adds to the uncertainty in obtaining the H_2O diffusivity, the effect is expected to be small. The diffusivity is primarily constrained by the length of the diffusion profile. Furthermore, our data for different $H_2O_{t,i}$ contents at same pressure and temperature conditions give consistent $D_{H_2O_m}$.

Second, the change in IR baseline shape indicates change either in Fe^{2+} environment and/or in Fe^{3+}/Fe^{2+} ratio. The change occurred throughout each sample and in samples from experiments under both reducing and oxidizing conditions (Fig. 4). Hence, the change in background does not seem to indicate oxidation or reduction. Keppler (1992) suggests that the Fe^{2+} absorption peaks in Ab_{100} and $Ab_{50}Di_{50}$ glasses at 5260–5400 and 9090–9260 cm^{-1} are due to different coordination of Fe^{2+}. Thus, change in the coordination number of Fe^{2+} may cause the disappearance of the 5600 cm^{-1} peak. However, the change in Fe^{2+} environment would not affect H_2O diffusivity. On the other hand, we do not expect a large effect of Fe^{3+}/Fe^{2+} ratio on inferred diffusivity. Diffusion experiments at low T in both CSVs were under relatively more reducing conditions than original sample. The 1-bar experiment (sample DC53B3) was under more oxidizing conditions. Nonetheless, H_2O diffusivity from experiment DC53B3 is consistent from data from more reducing experiments (Fig. 3). The possible change in hydrogen content imposed by reducing of Fe^{3+} is small. Because the final H_2O_t content in the center region of each sample is not significantly less than $H_2O_{t,i}$, reduction of H_2O to H_2 does not play a significant role in the H_2O diffusion profile.

Another uncertainty in H_2O diffusivity is caused by bubbles but is also expected to be small. Small bubbles (~0.7 μm) uniformly distributed in samples with H_2O_t>0.8 wt.% (DC2 and DC1) after the diffusion experiments (see Table 2). These bubbles are not caused by water oversaturation because experimental pressure in the CSV-1 and CSV-2 was above the saturation pressure of water and was roughly constant. One likely explanation is that they are air and/or CO_2 bubbles. Because all original samples were synthesized by fusing powder at 5 kbars, the dissolved air content may vary depending on the packing of powder. Hence, at our experimental conditions (~1 kbar), the sample could be oversaturated with respect to total volatile content (air+CO_2+H_2O) and there could be gas exsolution from the sample. The solubility of N_2 at 1 kbar is ~100 ppm in hydrous albitic melt and basaltic melt (Carroll and Webster, 1994). Because (i) these bubbles are not interconnected and their volume fraction is very small, (ii) measured H_2O_t after diffusion experiment in the center portion of the sample unaffected by diffusion does not decrease

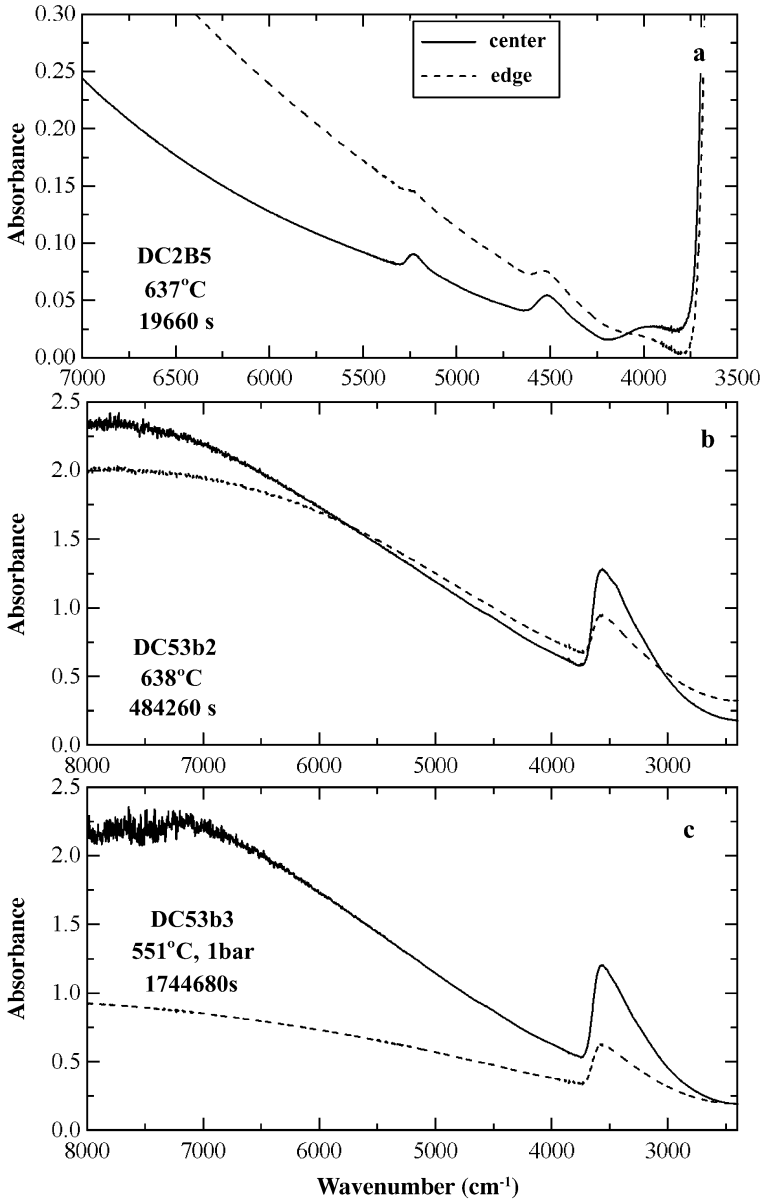

Fig. 4. FTIR spectra of several samples scaled to a thickness of 0.1 mm. Note the difference in the scale of *x*- and *y*-axis.

compared to the initial H_2O_t, and (iii) D_0 values from samples without bubbles and those from samples containing bubbles fall on the same trend, the small bubbles are not expected to significantly affect the extracted H_2O diffusivity.

With these uncertainties in mind, the actual uncertainty in calculated ln $D_{H_2O_t}$ using Eq. (7) is probably about 0.5 in the temperature and H_2O_t range covered by our experiments, instead of the fit error of 0.22.

4.3. Comparison with H_2O diffusion in other melts

Compared with rhyolitic melt at $H_2O_t \leq 2.5$ wt.%, $D_{H_2O_t}$ in dacitic melt increases more rapidly with H_2O_t at 500–640 °C (e.g. 600 °C, Fig. 5). $D_{H_2O_t}$ is

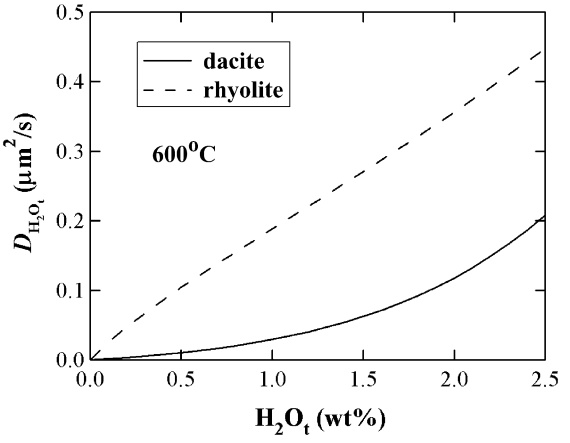

Fig. 5. $D_{H_2O_t}$ in dacitic and rhyolitic melts plotted against H_2O_t at 600 °C.

proportional to H_2O_t content in dacitic melt only at H_2O_t<0.8 wt.%, whereas in rhyolitic melt the relation holds for H_2O_t≤2 wt.%.

The diffusion of H_2O in melts of different compositions may also be compared in a ln $D_{H_2O_t}$ vs. $1/T$ plot (Fig. 6). The diffusion of H_2O in rhyolitic melt has been investigated at a wide range of temperature (400–1200 °C) and pressure (1–8100 bars) with 0.1–7.7 wt.% H_2O_t (Zhang et al., 1991; Zhang and Behrens, 2000). The calculated $D_{H_2O_t}$ for dacite from Eq. (7) is compared with values for rhyolite from Zhang and Behrens (2000). At 551–637 °C, $D_{H_2O_t}$ in dacitic samples is lower than those in rhyolitic samples by a factor of 2–2.5 for 2.5 wt.% H_2O_t and a factor of 6–12 for 0.8 wt.% H_2O_t. The activation energies of $D_{H_2O_t}$ in dacite with 2.5 and 0.8 wt.% H_2O_t are 124 and 140 kJ/mol, respectively, greater than those in rhyolite (87 and 91 kJ/mol) with similar H_2O_t. Thus, extrapolation of the dacite diffusivity to higher T for samples with 2.5 wt.% H_2O_t suggests that H_2O diffusion in dacite is faster than that in rhyolite at T>740 °C (Fig. 6) with the intersection point depending on water content (about 730 °C for 0.8 wt.% H_2O and about 740 °C at 2.5 wt.% H_2O). Experimental data on H_2O diffusion in basaltic melt only cover 1.0 GPa, 1300–1500 °C and <0.4 wt.% H_2O_t (Zhang and Stolper, 1991). Hence, comparing diffusion in basaltic melt and dacitic melt requires large extrapolations of basaltic data. At 551–637 °C and for 0.8 wt.% H_2O_t, $D_{H_2O_t}$ in dacitic melt is about a factor of ~20 smaller than extrapolated $D_{H_2O_t}$ in basaltic melt (Zhang and Stolper, 1991). Experiments of H_2O diffusion in trachytic melt with 0.25–2 wt.% H_2O_t were also conducted at high pressure and temperature (1.0 GPa and 1000–1400 °C) (Freda et al., 2003). The activation energy of $D_{H_2O_t}$ (142 kJ/mol) in trachytic melt with 0.8 wt.% H_2O_t is similar to that in dacitic melt with same H_2O_t content. At 551–637 °C and for 0.8 wt.% H_2O_t, $D_{H_2O_t}$ in dacitic melt agrees with the extrapolated value in trachytic melt within error.

The slower diffusion rate of H_2O in dacitic melt than in rhyolitic melt at low temperatures might be counter-intuitive at first sight, because conventional wisdom is that diffusion and other kinetic processes in less-polymerized dacitic melt should be more rapid than in rhyolitic melt. However, the comparison we have made is for undercooled melt near the glass transition, not the stable liquid. Moreover, the slower H_2O diffusivity in dacitic melt than in rhyolitic melt at such low temperatures can be rationalized from the viscosity data. Although no viscosity data for dacitic melt are available, at 2.5 wt.% H_2O_t, the viscosity of less-polymerized andesitic melt (Richet et al., 1996) has been found to be greater than that of rhyolitic melt (Zhang et al., 2003) at T<610 °C. It is interesting to note that H_2O diffusivity decreases also strongly from

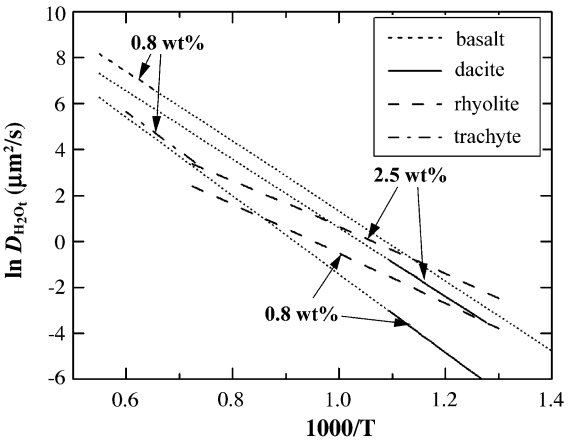

Fig. 6. Comparison of H_2O_t diffusivity in dacitic melt (solid lines) with those in basaltic melt (short dashed line, Zhang and Stolper, 1991), trachytic melt (dash dotted line, Freda et al., 2003) and rhyolitic melt (long dashed lines, Zhang and Behrens, 2000). Dotted lines are the extrapolated values from the diffusivity models of basalt and dacite, respectively.

$NaAlSi_3O_8$ (Ab) to $Ca_{0.5}AlSi_3O_8$ ($Qz_{50}An_{50}$) composition near the glass transition, e.g., by two orders of magnitude at 600 °C (Behrens and Schulze, 2000). Hence, introducing alkaline-earth elements in the melt structure appears to reduce the mobility of H_2O at least at low temperatures.

5. Conclusions

The diffusivity of H_2O was determined for hydrous dacitic melts at intermediate temperatures (551–637 °C) for H_2O_t<2.5 wt.%. Water diffusivity depends on water content. At $H_2O_t \leq 0.8$ wt.%, H_2O diffusivity is proportional to the water content. At higher water contents, H_2O diffusivity increases exponentially with H_2O_t contents. The diffusivity of H_2O_t can be expressed as:

$$D_{H_2O_t} = X\exp[20.463 - 40.433X + (-18,106 + 69,230X)/T]$$

where T is in Kelvin and X is the mole fraction of H_2O_t on a single oxygen basis. This equation reproduces the experimental ln $D_{H_2O_t}$ to within 0.22, but a more realistic total error assessment by considering other experimental uncertainties is 0.5 in ln $D_{H_2O_t}$. At 550–650 °C, water diffuses more slowly in dacitic melts than in rhyolitic melts.

However, the activation energies of $D_{H_2O_t}$ in dacite (124 kJ/mol at 2.5 wt.% H_2O_t and 140 kJ/mol at 0.8 wt.% H_2O_t) are greater than those in rhyolite (87 and 91 kJ/mol). Thus, the extrapolation of the above equation to T>740 °C for samples with 2.5 wt.% H_2O_t is greater than that in rhyolite at higher temperatures. The calculated bubble growth in dacite and rhyolite shows that bubbles grow slower in dacite than in rhyolite at a temperature close to that of lava domes (700 °C). This result may have important implications for the collapse of dacitic domes into pyroclastic flows.

Acknowledgements

This work was supported by US NSF grants INT-9815351, EAR-9972937, EAR-0106718 and EAR-0125506 and by the DFG grants Ho1337/3 and Ho1337/7. We thank Susanne Ohlhorst for providing anhydrous dacitic samples, Melanie Sierralta and Astrid Tegge-Schüring for helping with the internally heated pressure vessel, Hejiu Hui for sharing unpublished data for quench rate of CSV-2, and Otto Diedrich for preparation of some doubly polished samples and microprobe samples. We also thank James Mungall, Alan Whittington and Sumit Chakraborty for their thorough and constructive reviews. **[RR]**

References

Behrens, H., Schulze, F., 2000. Compositional dependence of water diffusion in aluminosilicate glasses and melts. In: Rammlmair, D., Mederer J., Oberthür, Th., Heimannund, R.B., Petinghaus, H. (Eds.), Applied Mineralogy in Research, Economy, Technology and Culture, Proc. 6th Int. Conf. Appl. Mineral, vol. 1. Balkema, Rotterdam, pp. 95–98.

Behrens, H., Zhang, Y., 2001. Ar diffusion in hydrous silicic melts: implications for volatile diffusion mechanisms and fractionation. Earth Planet. Sci. Lett. 192, 363–376.

Berndt, J., Holtz, F., Koepke, J., 2001. Experimental constraints on storage conditions in the chemically zoned phonolitic magma chamber of the Laacher See volcano. Contrib. Mineral. Petrol. 140, 469–486.

Berndt, J., Liebske, C., Holtz, F., Freise, M., Nowak, M., Ziegenbein, D., 2002. A combined rapid-quench and H2-membrane setup for internally heated pressure vessels: description and application for water solubility in basaltic melts. Am. Mineral. 87, 1717–1730.

Carroll, M.R., Webster, J.D., 1994. Solubility of sulfur, noble gases, nitrogen, chlorine, and fluorine in magmas. Rev. Miner. 30, 231–279.

Delaney, J.R., Karsten, J.L., 1981. Ion microprobe studies of water in silicate melts: concentration-dependent diffusion in obsidian. Earth Planet. Sci. Lett. 52, 191–202.

Doremus, R.H., 1962. Structural information from transport measurements in glass. Phys. Chem. Glasses 3, 127–128.

Doremus, R.H., 1983. Diffusion-controlled reaction of water with glass. J. Non-Cryst. Solids 55, 143–147.

Freda, C., Baker, D.R., Romano, C., Scarlato, P., 2003. Water diffusion in natural potassic melts. In: Oppenheimer, C., Pyle, D.M., Barclay, J. (Eds.), Volcanic Degassing, Geol. Soc. London Special Publication, vol. 213. London Geological Society, pp. 52–62.

Friedman, I., Long, W., 1976. Hydration rate of obsidian. Science 191, 347–352.

Karsten, J.L., Holloway, J.R., Delaney, J.R., 1982. Ion microprobe studies of water in silicate melts: temperature-dependent water diffusion in obsidian. Earth Planet. Sci. Lett. 59, 248–420.

Keppler, H., 1992. Crystal field spectra and geochemistry of transition metal ions in silicate melts and glasses. Am. Mineral. 77, 62–75.

Lapham, K.E., Holloway, J.R., Delaney, J.R., 1984. Diffusion of H_2O and D_2O in obsidian at elevated temperatures and pressures. J. Non-Cryst. Solids 67, 179–191.

Liu, Y., Zhang, Y., Behrens, H., 2004a. Solubility of H_2O in rhyolitic melts at low pressures and a new empirical model for mixed H_2O–CO_2 solubility in rhyolitic melts. J. Volcanol. Geotherm. Res. (submitted for publication).

Liu, Y., Behrens, H., Zhang, Y., 2004b. The speciation of dissolved H_2O in dacitic melt. Am. Mineral. 89, 277–284.

Nakada, S., Motomura, Y., 1999. Petrology of the 1991–1995 eruption at Unzen: effusion pulsation and groundmass crystallization. J. Volcanol. Geotherm. Res. 89, 173–196.

Nowark, M., Behrens, H., 1997. An experimental investigation on diffusion of water in haplogranitic melts. Contrib. Mineral. Petrol. 126, 365–376.

Ohlhorst, S., Behrens, H., Holtz, F., 2001. Compositional dependence of molar absorptivities of near-infrared OH- and H_2O bands in rhyolitic to basaltic glasses. Chem. Geol. 174, 5–20.

Richet, P., Lejeune, A.M., Holtz, F., Roux, J., 1996. Water and the viscosity of andesite melts. Chem. Geol. 128, 185–197.

Rossman, G.R., 1984. Spectroscopy of Micas. In: Bailey, S.W. (Ed.), Micas, Reviews in Mineralogy, Washington, D.C., vol. 13, pp. 145–181.

Shaw, H.R., 1974. Diffusion of H_2O in granitic liquids: I. Experimental data and II. Mass transfer in magma chambers. In: Hofmann, A.W., et al., (Eds.), Geochem. Transport and Kinetics. Carnegie Institution of Washington, Washington, DC, pp. 139–170.

Swanson, S.E., Nye, C.J., Miller, T.P., Avery, V.F., 1994. Geochemistry of the 1989–1990 eruption of Redoubt Volcano: Part II. Evidence from mineral and glass chemistry. J. Volcanol. Geotherm. Res. 62, 453–468.

Whittington, A., Richet, P., Linard, Y., Holtz, F., 2001. The viscosity of hydrous phonolites and trachytes. Chem. Geol. 174, 209–224.

Wolf, K.J., Eichelberger, J.C., 1997. Syneruptive mixing, degassing, and crystallization at Redoubt Volcano, eruption of December, 1989 to May 1990. J. Volcanol. Geotherm. Res. 75, 19–37.

Yamashita, S., Kitamura, T., Kusakabe, M., 1997. Infrared spectroscopy of hydrous glasses of arc magma compositions. Geochem. J. 31, 169–174.

Zhang, Y., 1999. H_2O in rhyolitic glasses and melts: measurement, speciation, solubility, and diffusion. Rev. Geophys. 37, 493–516.

Zhang, Y., Behrens, H., 2000. H_2O diffusion in rhyolitic melts and glasses. Chem. Geol. 169, 243–262.

Zhang, Y., Stolper, E.M., 1991. Water diffusion in a basaltic melt. Nature 351, 306–309.

Zhang, Y., Stolper, E.M., Wasserburg, G.J., 1991. Diffusion of water in rhyolitic glasses. Geochim. Cosmochim. Acta 55, 441–456.

Zhang, Y., Belcher, R., Ihinger, P.D., Wang, L., Xu, Z., Newman, S., 1997. New calibration of infrared measurement of dissolved water in rhyolitic glasses. Geochim. Cosmochim. Acta 61, 3089–3100.

Zhang, Y., Xu, Z., Behrens, H., 2000. Hydrous species geospeedometer in rhyolite: improved calibration and application. Geochim. Cosmochim. Acta 64, 3347–3355.

Zhang, Y., Xu, Z., Liu, Y., 2003. Viscosity of hydrous rhyolitic melts inferred from kinetic experiments, and a new viscosity model. Am. Mineral. 88, 1741–1752.